Available online at www.sciencedirect.com
SCIENCE DIRECT®
Journal of Catalysis 222 (2004) 238–249
JOURNAL OF CATALYSIS
www.elsevier.com/locate/jcat

# Pd/Mg(Al)O catalysts obtained from hydrotalcites: investigation of acid–base properties and nature of Pd phases

Federica Prinetto,[a] Maela Manzoli,[a] Giovanna Ghiotti,[a,*] Maria de Jesus Martinez Ortiz,[b] Didier Tichit,[b] and Bernard Coq [b]

[a] *Dipartimento di Chimica IFM, Università di Torino, Via P. Giuria 7, 10125 Torino, Italy*
[b] *CNRS-ENSCM UMR 5618, 8 Rue de l'Ecole Normale, 34000 Montpellier, France*

Received 28 July 2003; revised 7 October 2003; accepted 21 October 2003

**Abstract**

A series of palladium catalysts with Pd loading in the range 0.05–1.5 wt% were prepared by impregnation with either Pd acetylacetonate or Pd chloride of Mg(Al)O mixed oxides obtained by thermal decomposition of hydrotalcite compounds. For comparative purposes, Pd catalysts supported on MgO and $Al_2O_3$ were prepared using the same procedures. The morphology of Pd particles was studied by TEM and HRTEM, while the surface acid–base properties, on the one hand, and the nature of Pd phases and the metal–support interactions, on the other hand, were investigated by FT-IR spectroscopy, using $CH_3CN$ and CO probes, respectively. Pd catalysts obtained by the acetylacetonate precursor exhibited strongly basic oxygen ions, similar to those of MgO, along with $Al^{3+}$ Lewis acid sites. A peculiarity of these catalysts was the presence of Pd sites, isolated or in very small clusters, strongly interacting with the basic oxygen anions of the support, which give carbonyl species showing unusual features. These sites were partially or totally depleted, depending on the amount of remaining Cl, on catalysts prepared with the chloride precursor.


*Keywords:* Palladium catalysts; Hydrotalcite; FT-IR spectroscopy; Acetonitrile; Carbon monoxide

## 1. Introduction

Hydrotalcite-type layered double hydroxides of general formula $[M^{II}_{1-x}M^{III}_x(OH)_2]^{x+}[A^{n-}_{x/n}] \cdot mH_2O$ (HT) display a lamellar structure consisting of brucite-like layers and compensating anions situated in the interlayer space [1,2]. Upon controlled thermal treatments, HT compounds decompose to $M^{II}(M^{III})O$ mixed oxides exhibiting high specific surface areas, homogeneous interdispersion, and synergetic effects between the elements [2–7]. These two materials exhibit attractive properties as precursors for redox catalysts with metal function, which were described in recent reviews [8,9]. Metal–support interaction [10,11] and metal–support cooperation (metal–base bifunctional catalysis) were put forward to interpret the reactivity for the partial oxidation of methane [12,13], the highest selectivity in the hydrogenation of phenol to cyclohexanone on Pd/Mg(Al)O [14], of acetylene to ethylene on LDH-derived Ni catalysts [6], of acetonitrile to ethylamine, and adiponitrile to aminocapronitrile on Ni/Mg(Al)O [15,16], as well as in the aromatization of *n*-hexane on Pt,Pd/Mg(Al)O [17], and in the "one-pot" synthesis of methylisobutylketone from acetone on Pd/Mg(Al)O [18–20]. These are few and rare examples showing very unique properties of metal/basic-support catalysts. Chemical composition, synthesis procedure, compensating anions, activation protocol, etc., all influence the textural and acid–base properties of HT compounds and of HT-derived mixed oxides [21,22], the structural and electronic properties of the metal function, and the nature of the metal–support interaction [10,23]. There is, however, a lack of fundamental studies to establish relationships between synthesis parameters, the general properties of the activated materials, and their behavior as redox catalysts. In this context, the investigation (i) of the acid–base properties and (ii) of the metal–support interaction and/or metal–support cooperation is of vital importance.

Hence, in this work we considered a series of Pd catalysts obtained by impregnation of HT-derived Mg(Al)O mixed oxides. The aim was to examine the influence of such para-

* Corresponding author.
*E-mail address:* giovanna.ghiotti@unito.it (G. Ghiotti).

0021-9517/$ – see front matter 
doi:10.1016/j.jcat.2003.10.014

meters as the nature of the Pd precursor (Pd acetylacetonate or Pd chloride), the Pd loading, and the sample pretreatment on the acid–base properties, on one hand, and on the nature of Pd phases and the metal–support interactions, on the other hand, by means of FT-IR spectroscopy, using acetonitrile and CO probes, respectively.

## 2. Experimental

### 2.1. Sample preparation

The HT compound was prepared by coprecipitation at pH $\approx$ 10 of suitable amounts of $Mg(NO_3)_2 \cdot 6H_2O$ and $Al(NO_3)_3 \cdot 6H_2O$ ($Mg^{2+}/Al^{3+} = 3$) with solutions of NaOH (1.0 M) + $Na_2CO_3$ ($2 \times 10^{-2}$ M). The addition of the alkaline solution and pH were controlled by pH-STAT Titrino (Metrohm). The suspension was stirred overnight at 353 K, and then the solid was separated by centrifugation, rinsed thoroughly with distilled water (Na < 100 ppm), and dried overnight at 353 K. The HT was heat-activated in air flow at 723 K for 4 h (heating rate: 2 K $min^{-1}$) to yield the Mg(Al)O mixed oxide.

Pd catalysts of different Pd loading were obtained by contacting the Mg(Al)O mixed oxide support for 12 h either with (i) water-free toluene solutions containing suitable amounts of Pd acetylacetonate, $Pd(acac)_2$ (Strem Chemicals) or (ii) $PdCl_2$ (Aldrich) aqueous HCl solutions (pH $\approx$ 2).

The solids were finally dried at 353 K ("as-prepared" samples) and calcined thereafter in air flow at 723 K for 4 h. Samples will be hereafter referred to as PdMgAl$x$(ac) and PdMgAl$x$(Cl), respectively, where $x$ is the nominal Pd content (wt%), ranging from 0.05 to 1.5 wt%, and (ac) or (Cl) indicates the impregnation with acetylacetonate or chloride precursors. For a sake of comparisons, reference $Pd/Al_2O_3$ and Pd/MgO catalysts were prepared following the same protocol as described above. The alumina support used was a commercial $\gamma$-$Al_2O_3$ (Rhône-Poulenc), while MgO was obtained by calcination at 723 K for 4 h of commercial $Mg(OH)_2$ (Strem Chemicals). These samples will be hereafter referred to as PdMg$x$(ac) or PdMg$x$(Cl) and PdAl$x$(ac) or PdAl$x$(Cl), respectively. The synthesis conditions and chemical compositions of all the prepared samples are summarized in Table 1.

### 2.2. Sample characterization

Chemical analysis of the samples as prepared or calcined at 723 K was performed at the Service Central d'Analyse du CNRS (Solaise, France).

XRD patterns of the samples as prepared or calcined at 723 K were recorded on a CGR Theta 60 instrument using Cu-$K_{\alpha 1}$ radiation ($\lambda = 1.542$ Å, 40 kV, and 50 mA).

$N_2$ sorption experiments at 77 K were carried out on samples previously calcined at 723 K and outgassed at 523 K ($10^{-4}$ Pa) with a Micromeritics ASAP2000 instrument. Specific surface areas were calculated using the BET method and are reported in Table 1.

Transmission electron microscopies (TEM) and high-resolution transmission electron microscopies (HRTEM) were taken with a JEOL 2000 EX electron microscope with a top entry stage, working at 200 kV and equipped with an EDS Oxford Link analytical system. The powdered materials, previously calcined at 723 K and reduced in $H_2$ at 673 K, were deposited on a copper grid coated with a holey carbon film. The instrumental magnification ranged from $2.5 \times 10^5$ to $8 \times 10^5$.

Absorption/transmission IR spectra were run at RT on a Perkin-Elmer FT-IR 1760-X spectrophotometer equipped with a Hg–Cd–Te cryodetector, working in the range of wavenumbers 7200–580 $cm^{-1}$ at a resolution of 2 $cm^{-1}$ (number of scans $\sim$ 50). For IR analysis, the calcined powders compressed in self-supporting pellets (10–12 mg $cm^{-2}$) were activated by heating under vacuum at increasing temperature up to 723 K (873 K in some cases), then submitted to redox cycles consisting of (i) reduction in pure $H_2$ at 673 K for 30 min and subsequent evacuation at the same temperature, and (ii) heating in dry $O_2$ at 723 K and cooling down to RT in oxygen. $CH_3CN$ (Carlo Erba, RPE) and CO (Matheson, C.P.) were used to characterize the acid–base properties and the metallic phases, respectively. All the spectra were reported as the difference between those recorded after and before the gas admission and normalized to the same pellet density.

## 3. Results and discussion

### 3.1. Structural and chemical characterization

Fig. 1 shows the XRD patterns of two representative samples of similar Pd loading (0.2 wt%) obtained using either $Pd(acac)_2$ or $PdCl_2$. Significant differences were observed by comparing the spectra of the as-prepared samples (Fig. 1a). Indeed, the PdMgAl0.2(ac) sample showed an XRD pattern characteristic of poorly crystallized Mg(Al)O mixed oxides with a rock salt structure [2,24], whereas PdMgAl0.2(Cl) showed peaks of the HT structure (JCPDS file No. 14-191) in addition to those of Mg(Al)O. This latter feature accounts for the partial reconstruction of the lamellar network occurring during the impregnation of mixed oxide with the aqueous $PdCl_2$ solutions [1]. Conversely, the mixed oxide structure was preserved during the impregnation with the water-free toluene solutions of $Pd(acac)_2$.

After calcination at 723 K both samples showed similar XRD patterns, characteristic of poorly crystallized Mg(Al)O mixed oxides, showing a similar structure as periclase MgO with partial substitution of $Mg^{2+}$ by $Al^{3+}$ cations (Fig. 1b).

As expected, XRD patterns of the calcined PdMgAl$x$ samples were very similar to those of MgO-supported reference sample (Fig. 1b, curve 3).

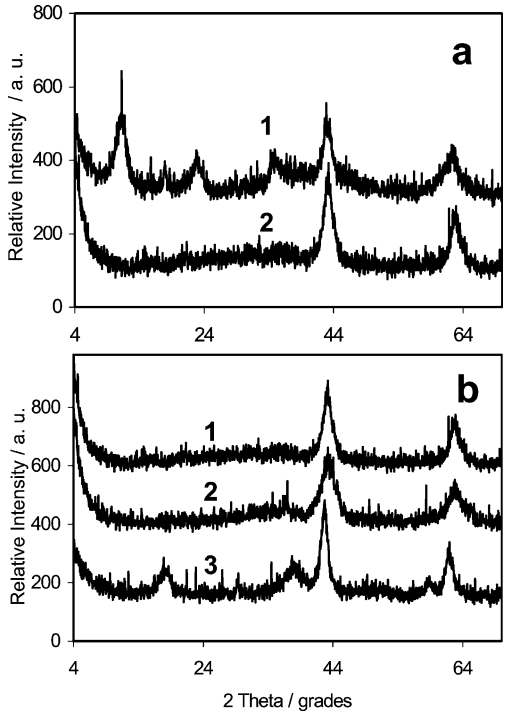


Fig. 1. XRD patterns of Pd samples as prepared (a) and thereafter calcined at 723 K (b). PdMgAl0.2(Cl) (curves 1); PdMgAl0.2(ac) (curves 2); PdMg0.2(ac) (curve 3).

XRD patterns of all the calcined samples remained unchanged after reduction, no diffraction line of $Pd^0$ could be detected.

The specific surface areas of the calcined samples are reported in Table 1. PdMgAl$x$(Cl) samples showed slightly lower specific surface areas in comparison to PdMgAl$x$(ac) with similar Pd loading. This was possibly due to the effects of the impregnation with the acidic $PdCl_2$ solutions on the basic Mg(Al)O support, e.g., dissolution of small particles and reprecipitation of larger ones.

Residual chlorine was found on as-prepared samples obtained by impregnation from $PdCl_2$ in amounts depending on the oxide support. Specifically, very small Cl amounts were retained in the case of the MgO-supported sample. Interestingly, the Mg(Al)O mixed oxide exhibits higher capacity than alumina for retaining chlorine though possessing a relatively low Al content ($Mg^{2+}/Al^{3+} = 3$). Upon calcination in air at 723 K, a large proportion of chlorine (40–50%) was eliminated for Mg(Al)O-supported samples, while the decrease was much smaller (around 6%) for the alumina-supported one. The amounts of chlorine still present in the calcined PdMg0.2(ac) sample were negligible. These behaviors could be explained as follows. MgO and $Al_2O_3$ are well below their points of zero charge under the acidic conditions ($pH \approx 2$) used for the impregnation with $PdCl_2$ and are thus able to retain $PdCl_4^{2-}$ species which prevail at these pH values, along with $Cl^-$ anions. The low Cl amounts found in the as-prepared MgO-supported samples indicate that Cl is almost completely eliminated as HCl already during the drying at 353 K, thus leading to the formation of a Cl-free supported PdO phase. Conversely, the high Cl amounts in the case of alumina-supported samples can account for the easy exchange of chloride anions with the weakly basic $OH^-$ sites of the alumina during the impregnation and calcination processes. Chlorine associated with both the support and the Pd phases is thus expected to be present in the calcined samples. Chlorided Pd species have been indeed observed by Mahata and Vishwanathan [25] on calcined $PdCl_2/Al_2O_3$ systems.

Mg(Al)O exhibits a specific behavior. The impregnation with $PdCl_2$ in aqueous HCl solutions is accompanied by a reconstruction of the mixed oxide in its lamellar form as previously shown by XRD. Therefore some $Cl^-$ anions are retained as compensating anions in the interlayer space of the lamellar structure; therefore, significant Cl amounts remain in the mixed oxide lattice.

### 3.2. Acid–base properties

The surface acid–base properties of the bare supports and of Pd-containing catalysts were studied using an acetonitrile probe, followed by FT-IR spectroscopy. Indeed, this amphoteric molecule is fully adapted for investigating the nature,

Table 1
Synthesis condition, chemical composition, and specific surface areas (SS) of the different Pd catalysts

| Sample | Pd precursor | Pd content[a] | | Cl content (wt%) | | SS[a] |
|---|---|---|---|---|---|---|
| | | wt% | at. $nm^{-2}$ | As prepared | Calcined[a] | ($m^2\,g^{-1}$) |
| PdMgAl0.05(ac) | $Pd(acac)_2$ | 0.05 | 0.012 | – | – | 230 |
| PdMgAl0.2(ac) | $Pd(acac)_2$ | 0.20 | 0.049 | – | | 230 |
| PdMgAl0.5(ac) | $Pd(acac)_2$ | 0.51 | 0.131 | – | – | 220 |
| PdMgAl1.5(ac) | $Pd(acac)_2$ | 1.51 | 0.485 | – | – | 176 |
| PdMgAl0.2(Cl) | $PdCl_2$ | 0.20 | 0.055 | 2.02 | 0.92 | 204 |
| PdMgAl1.2(Cl) | $PdCl_2$ | 1.22 | 0.460 | 2.71 | 1.55 | 150 |
| PdMg0.2(ac) | $Pd(acac)_2$ | 0.19 | 0.041 | – | – | 260 |
| PdMg1.5(ac) | $Pd(acac)_2$ | 1.48 | 0.347 | – | – | 240 |
| PdMg0.2(Cl) | $PdCl_2$ | 0.15 | 0.029 | 0.081 | 0.041 | 290 |
| PdAl0.2(ac) | $Pd(acac)_2$ | 0.21 | 0.044 | – | – | 270 |
| PdAl0.2(Cl) | $PdCl_2$ | 0.23 | 0.048 | 1.53 | 1.43 | 268 |

[a] Determined on samples calcined at 723 K

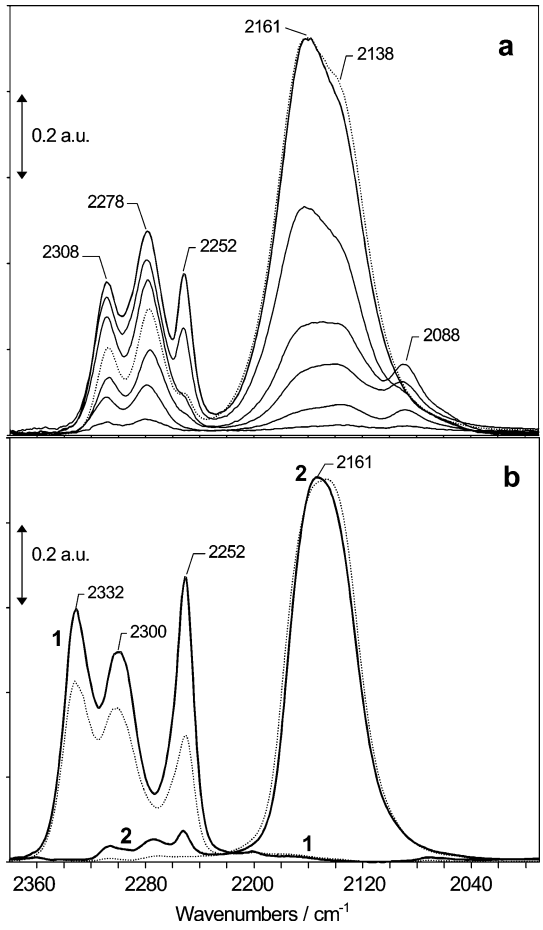


Fig. 2. IR spectra upon adsorption of $CH_3CN$. (a) Admission of $CH_3CN$ at increasing doses up to 200 Pa on Mg(Al)O mixed oxide. (b) Admission of $CH_3CN$ (200 Pa) on $Al_2O_3$ (curve 1) and MgO (curve 2). Dotted lines: subsequent evacuation at RT. Each spectrum is reported after subtraction of the spectrum before $CH_3CN$ interaction.

the strength, and the amount of the surface Lewis or Brønsted basic and acid sites.

$CH_3CN$ interaction with the Pd-free oxide supports was first examined. Fig. 2 shows the spectra upon acetonitrile admission on Mg(Al)O mixed oxide and on the reference MgO and $Al_2O_3$ oxides. The spectra are reported in a restricted range (2400–2000 $cm^{-1}$), characteristic of $\nu(C{\equiv}N)$ modes, because all the surface species formed exhibited vibrational modes in this region.

In the 2360–2230 $cm^{-1}$ region, i.e., characteristic of species formed on Lewis acid sites, the spectra of Mg(Al)O (Fig. 2a) exhibited a couple of bands at 2308 and 2278 $cm^{-1}$, which can be assigned to the $\nu$(CN) fundamental mode of acetonitrile N-bonded to Lewis acid sites ($Al^{3+}$), split by coupling with the $\nu(CC) + \delta_{sym}(CH_3)$ combination [26]. As known, the blue shift of these bands with respect to liquid acetonitrile (2292, 2254 $cm^{-1}$) depends on the electron withdrawing power of the cationic site and can be taken as a measure of the Lewis acidity [27,28]. In the case of pure alumina (Fig. 2b, curve 1) the couple of bands due to coordinated acetonitrile exhibited a higher frequency (2332, 2300 $cm^{-1}$) and intensity. These findings are evidence that $Al^{3+}$ sites in the mixed oxide possess lower acidic strength than on alumina, possibly suffering the effects of the surrounding MgO-type matrix, and are obviously present in lower amounts. A third component at 2252 $cm^{-1}$, observed at high $CH_3CN$ coverages, was associated both with physisorbed and H-bonded acetonitrile (the corresponding band expected around 2290 $cm^{-1}$ is overlapped to the modes of coordinated acetonitrile). Upon evacuation at RT (Fig. 2a, dotted line), physisorbed and H-bonded species were removed, together with a fraction of coordinated acetonitrile. On alumina, this band showed higher intensity and resistance at the evacuation at RT. This can be related to the presence of higher amounts of surface hydroxyl groups on alumina, and likely of higher acidity, able to give H-bonded acetonitrile species stable at RT. In the case of MgO (Fig. 2b, curve 2), the bands due to coordinated acetonitrile are very weak, shifted to lower frequency (2305, 2272 $cm^{-1}$), and almost completely removed by evacuation at RT. These findings account for the very low Lewis acidity of $Mg^{2+}$ sites.

The 2230–2050 $cm^{-1}$ spectral region is characteristic of the $\nu$(CN) modes of anionic species ($CH_2CN^-$ and/or polymeric anions) formed on strongly basic $O^{2-}$ sites and adsorbed thereafter onto the adjacent cationic sites [29,30]. Both Mg(Al)O and MgO exhibited intense absorptions around 2200–2100 $cm^{-1}$, whereas anionic species were not detected on alumina, accounting for the poor basicity of oxygen ions in $Al^{3+}O^{2-}$ pairs.

Upon admission of small doses of $CH_3CN$ on Mg(Al)O mixed oxides (Fig. 2a) and on MgO (not reported in the figure) a band at 2088 $cm^{-1}$ was observed but disappeared thereafter on increasing the $CH_3CN$ coverage. This band was assigned to $CH_2CN^-$ anions coordinated on $Mg^{2+}$ sites. Concurrently, an intense absorption with maximum at 2161 $cm^{-1}$ and a shoulder at 2138 $cm^{-1}$ developed. These bands were ascribed to polyanions coordinated mainly on $Mg^{2+}$ sites. The higher complexity of the absorption band on Mg(Al)O with respect to MgO can be ascribed to an increase of the heterogeneity of surface $Mg^{2+}O^{2-}$ pairs due to the presence of $Al^{3+}$ defects in the MgO lattice.

The spectra upon acetonitrile adsorption on supported Pd catalysts and subsequent evacuation at RT are reported in Fig. 3. No significant difference appeared between the bare support and the corresponding catalysts of low Pd content ($\leqslant$ 0.2 Pd wt%). Therefore, we can conclude that, for these Pd loadings, the impregnation with the acetylacetonate precursor does not modify the acid–base properties of the supports. For the PdMgAl1.5(ac) sample (Fig. 3a, curve 2), a significant decrease of the bands associated with both basic and acid sites was observed. This put in evidence a significant coverage of the support by the Pd oxide phase, which possesses evidently $Pd^{2+}O^{2-}$ pairs of weaker Lewis acid–base strength.

The effect of the Pd precursor is then examined. By comparing the spectra of PdMgAl0.2(ac) and PdMgAl0.2(Cl) samples (Fig. 3a, curves 1 and 3, respectively), it is worth

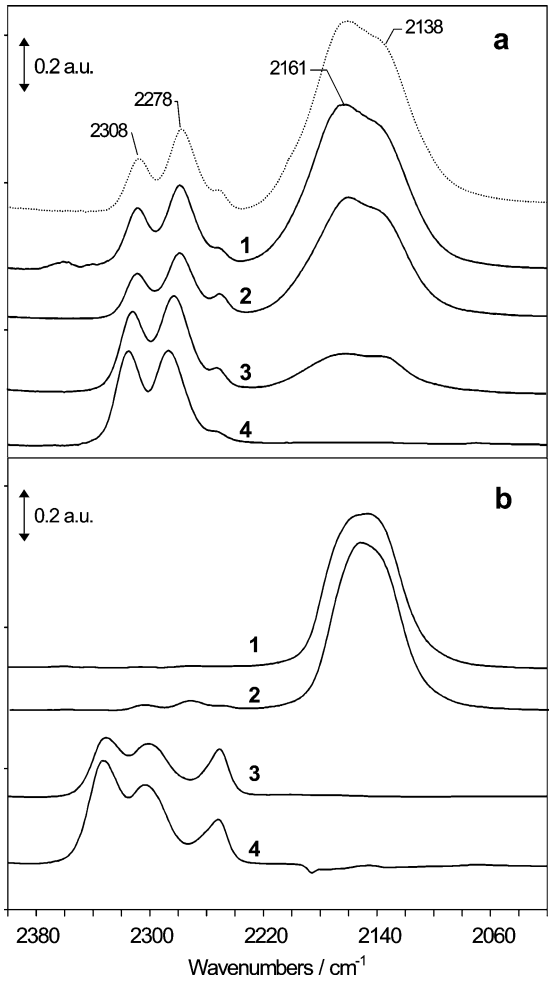


Fig. 3. IR spectra upon adsorption of $CH_3CN$ (200 Pa) and subsequent evacuation at RT on Pd catalysts oxidized at 723 K. (a) PdMgAl0.2(ac) (curve 1); PdMgAl1.5(ac) (curve 2); PdMgAl0.2(Cl) (curve 3); PdMgAl1.2(Cl) (curve 4). For comparison the spectrum of pure Mg(Al)O is reported (dotted line). (b) PdMg0.2(ac), (curve 1); PdMg0.2(Cl) (curve 2); PdAl0.2(ac) (curve 3); PdAl0.2(Cl) (curve 4). Each spectrum is reported after subtraction of the spectrum before $CH_3CN$ interaction and translated along the *Y* axis for the sake of clarity.

noting that the presence of chlorine sharply decreased the amount of basic sites, whereas the amount and the strength of the acid sites increased. The number and the strength of acid sites further increased on the PdMgAl1.2(Cl) sample, which contains larger amounts of chlorine; in this case the strongly basic $O^{2-}$, able to give the anionic species, completely disappeared (Fig. 3a, curve 4). These findings suggest that a fraction of chlorine replaces oxygen anions during the thermal decomposition of the HT material into the mixed oxide [31,32] and it was not removed during the subsequent oxidation–reduction treatments. Indeed, the spectra upon $CH_3CN$ adsorption on PdMgAl$x$(Cl) samples just calcined or thereafter submitted to reduction–oxidation cycles superimposed.

Concerning the reference catalysts, the comparison of PdMg0.2(ac) and PdMg0.2(Cl) samples (Fig. 3b, curves 1 and 2, respectively) showed only a slightly higher amount of acid sites in the latter, while the basic sites were almost unaffected. At variance, in the case of alumina-supported catalysts, the Lewis acidity markedly increased on going from the PdAl0.2(ac) to the PdAl0.2(Cl) sample (Fig. 3b, curves 3 and 4, respectively). Such behavior is consistent with the respective amounts of chlorine in these samples (see Table 1).

### *3.3. Nature of Pd phases and metal–support interaction*

The morphology of Pd particles over the Mg(Al)O and MgO supports was examined by TEM and HRTEM analysis of the prereduced samples.

The PdMgAl1.5(ac) catalyst showed Pd particles of spherical shape, which appeared as a dark contrast (Fig. 4a). The particle-size distribution ranged from 2 to 8 nm and the average diameter was 3.5 nm (Fig. 5a). No diffraction fringes were observed.

As for the PdMgAl0.5(ac) sample, the size distribution ranged from 1 to 4 nm and the average Pd particle size was 2.4 nm. On the contrary, no Pd particles could be detected on the samples with a Pd loading $< 0.5$ wt%, likely having sizes well below 2 nm (TEM images not shown).

The PdMg1.5(ac) sample (see Fig. 4b) exhibited Pd particles with an average diameter of 3.2 nm. This value is comparable to the one obtained for the Mg(Al)O-supported sample with the same Pd loading (3.5 nm). However, the particle-size distribution is narrower, ranging from 1.5 to 6 nm (Fig. 5b). It is also evident the different morphology of the MgO support, showing cubic crystallites with homogeneous size (around 2–3 nm of side), with respect to the Mg(Al)O support, exhibiting a poorly crystallized structure, in agreement with XRD results.

No Pd particles could be detected on MgO-supported samples with Pd loading $< 0.5$ wt%, similar to the observations previously made on Mg(Al)O-supported samples.

Finally, the comparison between PdMgAl1.5(ac) (Figs. 4a and 5a) and PdMgAl1.2(Cl) (Figs. 4c and 5c) revealed a deep influence of the Pd precursor used for the impregnation on the morphology of the metal particles. Indeed, the sample prepared with $PdCl_2$ showed Pd particles of larger average sizes (5.3 nm) and a broader particle-size distribution, ranging from 2 to 12 nm. Moreover, Pd particles on the PdMgAl1.2(Cl) sample clearly showed diffraction fringes with distances $d_{hkl}$ of 2.24 and 1.95 Å, corresponding to the (111) and (200) planes, respectively, of cubic Pd (JCPDS file No. 5-0683). An interesting finding is that EDS analysis (spectra not reported) revealed the presence of Cl all over the Mg(Al)O support and high Cl amounts were found particularly in the neighborhood of Pd particles.

The chemicophysical properties of Pd phases and the metal–support interaction were investigated by CO adsorption at RT, followed by IR spectroscopy. For this purpose, note that CO absorption bands on the bare supports (spectra not reported) are extremely weak so that they do not interfer with those associated to Pd. For the sake of clarity, the

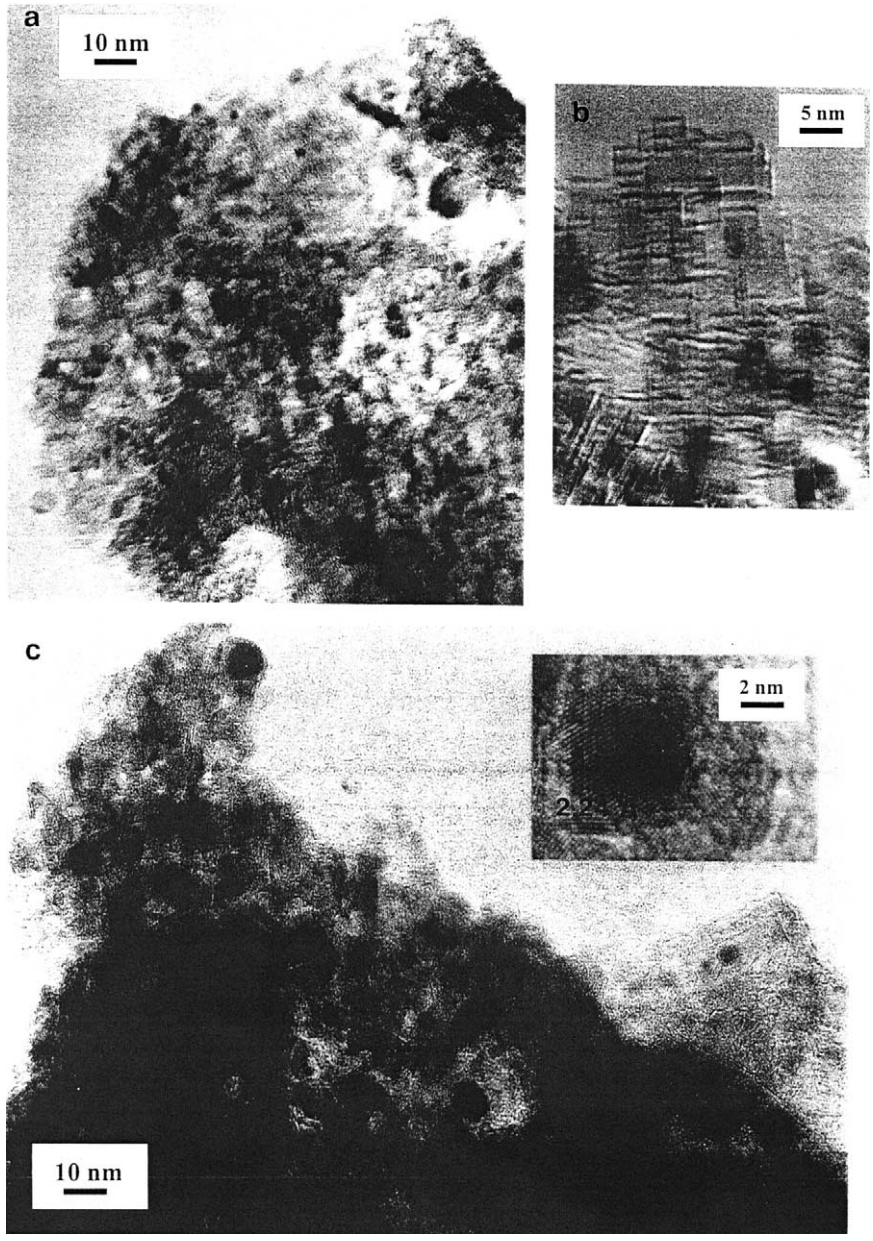


Fig. 4. TEM images of PdMgAl1.5(ac) (a), of PdMg1.5(ac) (b), and PdMgAl1.2(Cl) (c).

results concerning samples prepared by impregnation with $Pd(acac)_2$ or $PdCl_2$ are discussed separately in the following.

*3.3.1. Samples prepared by impregnation with $Pd(acac)_2$*

*3.3.1.1. Effect of the Pd loading* In Fig. 6 the spectra of CO adsorbed at increasing doses on PdMgAl1.5(ac) and PdMgAl0.5(ac) samples prereduced in $H_2$ at 673 K are reported. In both cases, complex absorptions bands were observed in the range 2100–2000 and 1970–1700 $cm^{-1}$. These bands are characteristic of linearly and bridge-bonded CO on $Pd^0$ atoms, respectively [33,34]. The observed spectral features are quite different with respect to those reported for CO adsorption at ca. 300 K on palladium single-crystal surfaces. Actually, in this case, bridge-bonded CO species prevail over a wide CO equilibrium pressure range [35–37]. In contrast, the ratio between linearly and bridged bonded species is high for PdMgAl$x$(ac) samples, as generally observed for polycrystalline Pd systems supported on various oxides [38–41]. In fact, the relative concentration of linear and bridged CO chemisorption sites is particle-size dependent, the former increasing at the expense of the latter on decreasing the Pd particle sizes [38,39]. This different behavior with respect to Pd single crystals is likely due to the presence of additional crystal facets and of higher amounts of low coordinated sites (terraces, edges, and corners) in polycrystalline systems.

Two main components at 1960 and 1880 $cm^{-1}$ were observed in the 1970–1700 $cm^{-1}$ region, the former being

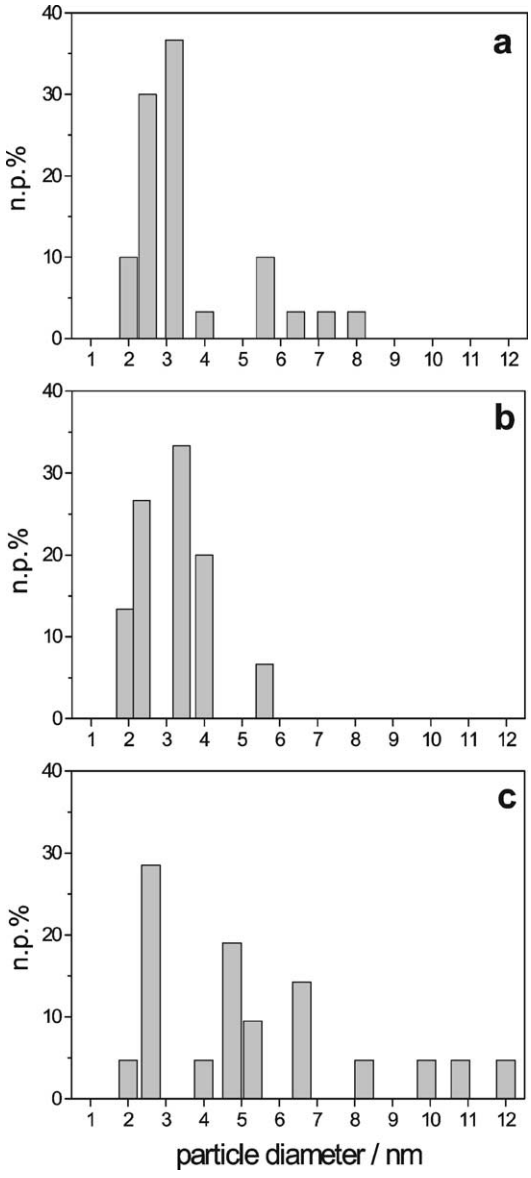


Fig. 5. Size distributions of Pd particles for the catalysts PdMgAl1.5(ac) (a), PdMg1.5(ac) (b), and PdMgAl1.2(Cl) (c) shown in the micrographs of Fig. 4.

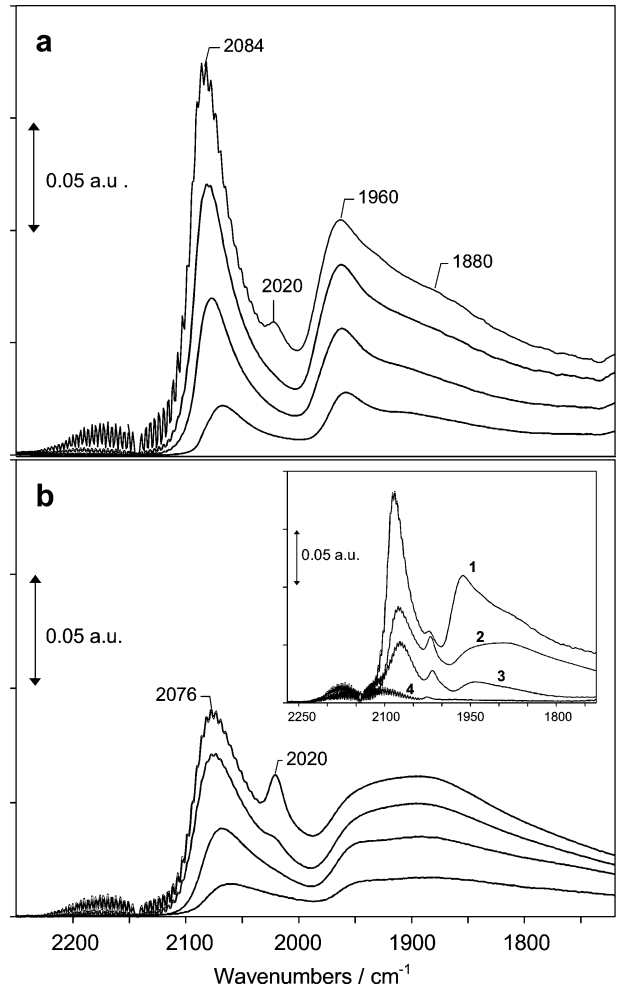


Fig. 6. Effect of the Pd loading. IR spectra upon adsorption of CO at increasing doses up to 2 kPa on PdMgAl1.5(ac) (a) and PdMgAl0.5(ac) (b), both reduced in $H_2$ at 673 K. (Inset of section b) Adsorption of CO (2 kPa) on reduced PdMgAl1.5(ac) (curve 1), PdMgAl0.5(ac) (curve 2), PdMgAl0.2(ac) (curve 3), and PdMgAl0.05(ac) (curve 4) samples. Each spectrum is reported after subtraction of the spectrum before CO admission.

prominent on the PdMgAl1.5(ac) sample. In agreement with the recent literature for Pd single crystals [34] the band at 1880 $cm^{-1}$ can be unambigously assigned to CO adsorbed on 3-fold hollow sites, while the band at 1960 $cm^{-1}$, classically assigned to 2-fold bridging sites on the Pd(100) face [35], can be assigned to 3-fold sites on the Pd(111) face. A minor component at 1705 $cm^{-1}$ (not reported in the figure), not observed for samples with Pd loadings < 1.5 wt%, is ascribed to multibridged CO species.

By examining the spectra of PdMgAl$x$(ac) samples with different Pd loading (see inset of Fig. 6b) it is noted that the bands of bridge-bonded CO decreased in intensity relatively to linear species on decreasing the Pd loading and were no more present on the PdMgAl0.05(ac) sample. This is evidence of an increasing Pd dispersion on the support.

A careful inspection of the spectra in the 2100–2000 $cm^{-1}$ region shows that the band of linearly bonded CO shifted from 2056 to 2084 $cm^{-1}$ ($\Delta\bar{\nu} = 28$ $cm^{-1}$) on PdMgAl1.5(ac) on increasing the CO pressure from 0.1 to 2000 Pa, but only from 2056 to 2076 $cm^{-1}$ ($\Delta\bar{\nu} = 20$ $cm^{-1}$) on the PdMgAl0.5(ac) sample. The shifts observed on increasing the CO coverage, due to dipole–dipole coupling, show that CO is linearly adsorbed on ordered aggregates of identical sites (same facet or terrace edge) rather than to isolated low-coordinated sites. The larger shift observed on the PdMgAl1.5(ac) than on the PdMgAl0.5(ac) sample indicates that the ordered aggregates of identical sites, and therefore the Pd particle sizes, are larger on the former sample, as confirmed by HRTEM analysis. However, CO-stretching frequencies found for on-top species on PdMgAl$x$(ac) catalysts are largely below those reported for Pd single crystals, accounting for the presence of small Pd cluster (< 4 nm),

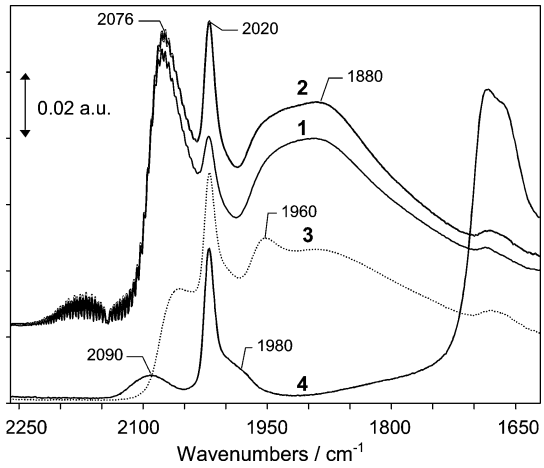


Fig. 7. IR spectra upon CO interaction on PdMgAl0.5(ac) catalyst reduced in $H_2$ at 673 K: admission of 2 kPa of CO, spectrum recorded after 1 min (curve 1) and 10 min of contact (curve 2), and subsequent evacuation at RT (curve 3), and subsequent admission of $O_2$ (2 kPa) at RT (curve 4). Each spectrum is reported after subtraction of the spectrum before CO admission and translated along the *Y* axis for the sake of clarity.

in agreement with HRTEM data, which are known to give stronger chemisorption bonds [42,43].

A further component at 2020 $cm^{-1}$ was observed on all the PdMgAl samples and it was particularly intense on those with Pd loading in the range 0.2–0.5 wt% (see inset of Fig. 6b). This band exhibited peculiar features such as a low frequency but still in the range characteristic of linearly bonded species, low rate of formation, and high stability. Indeed, it appeared only at high CO coverage and it increased in intensity on increasing the contact time with CO (Fig. 7, curves 1 and 2). Moreover, it was not affected by evacuation at RT (Fig. 7, curve 3) and it was removed only by heating under vacuum at 523 K (not reported). Finally, the carbonyl species associated with the band at 2020 $cm^{-1}$ was not affected by oxygen admission at RT (Fig. 7, curve 4). In contrast, all the other carbonyl species almost completely disappeared (only weak bands around 2090 and 1980 $cm^{-1}$ were still detected) and carbonates were formed concurrently, accounting for the oxidation of adsorbed CO species. Similar features have been scarcely reported in the literature. A band at 2010 $cm^{-1}$ has been observed for reduced $Pd/CeO_2$ and ascribed to CO linearly bonded to a Pd atom in an electron-donor oxygen vacancy [44]. Unusual properties have also been reported for CO adsorbed on Pt/Mg(Al)O [10,23]. In particular, Kazansky et al. [23] attributed to the presence of Pt particles encapsulated between the hydrotalcite layers a band at 2012 $cm^{-1}$ showing low frequency, low rate of formation, and high stability. They also suggested that Pt could be additionally modified by charge-compensating anions. However, if the first hypothesis is sustainable, since the decomposition of the layered structure occurs topotactically [21,45], the presence of anions after thermal treatments at 673 K is more questionable. As a matter of fact, in the samples studied here no reconstruction of the hydrotalcite structure occurs during the impregnation with $Pd(acac)_2$ in water-free toluene solutions. As a consequence, a trapping of Pd could hardly occur. Gandao et al. [10] observed on Pt/Mg(Al)O samples a band exhibiting low frequency and high thermal stability, which was ascribed to CO adsorbed on Pt sites strongly interacting with the basic sites of the support. They also suggested that this band could be due to CO bridge bonding between peripherical Pt sites and $Mg^{2+}$ cations. We agree with the first suggestion, so we assign the band at 2020 $cm^{-1}$ to CO linearly bonded to Pd sites with electronic properties strongly changed by interaction with basic oxide ions of the support. The increased back-donation to $2\pi^*$ antibonding orbitals of CO, responsible for the frequency red shift, can be interpreted as a result of an electron-density transfer from the oxide ions to the Pd sites. Alternatively, it can result from a decrease in the ionization potential of the Pd valence orbitals, directly induced by the Coulomb potential of the oxygen ions [46,47]. The large red shift of this band (around 120 $cm^{-1}$) with respect to gaseous CO is evidence that the metal–support interaction is very strong and suggests that Pd sites are isolated or belong to very small Pd clusters. The involvement of strongly basic oxide ions is also supported by the experiments carried out on MgO and $Al_2O_3$-supported reference catalysts (see infra in Fig. 9). It is worth noting that a component at 2015 $cm^{-1}$ is also present in the case of the MgO-supported samples. This component shows behavior analogous to the band at 2020 $cm^{-1}$ observed on PdMgAl$x$(ac) samples, and it is therefore assigned to carbonyls formed on Pd sites, isolated or belonging to very small clusters and interacting with strongly basic $O^{2-}$ sites of the MgO support. At variance, as expected, no peaks in this position and with this behavior are observed for the alumina-supported catalysts. Till now, no experimental results about CO adsorbed on MgO-supported Pd samples show the formation of similar species. However, the assignment is supported by the density-functional cluster model calculations carried out by Abbet et al. [48], who estimated the CO vibrational frequency and the strength of the Pd–CO bond for CO on-top bound on isolated Pd atoms deposited on MgO(100). In the case of Pd(CO) complexes formed on Pd atoms interacting with coordinatively unsaturated $O^{2-}$ sites of the MgO substrate, they found CO adsorption energies in the range 2.2–2.6 eV and CO frequencies red-shifted of 140–170 $cm^{-1}$ with respect to the frequency of gaseous CO. These data are in agreement with the high stability and low vibrational frequency of the bands at 2020 and 2015 $cm^{-1}$. Finally, regarding the slow formation rate of the carbonyl species associated with the band at 2020 $cm^{-1}$ (2015 $cm^{-1}$ on MgO-supported samples), a change of Pd coordination upon CO adsorption, e.g., extraction of Pd from the matrix or disruption of Pd clusters, could be suggested, as already proposed for oxide-supported Pt [49].

*3.3.1.2. Effect of the sample pretreatment* The effect of the sample pretreatment, i.e., reduction in $H_2$ at 673 K or oxidation at 723 K, and the stability of the Pd phases upon

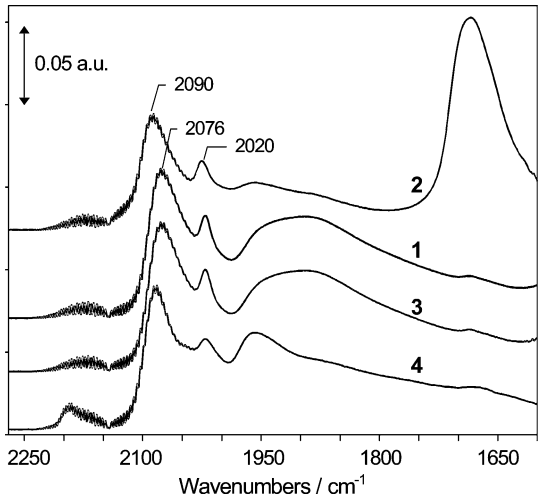


Fig. 8. Effect of the sample pretreatment. IR spectra upon adsorption of CO (2 kPa) on PdMgAl0.5(ac) reduced in $H_2$ at 673 K (curve 1), then oxidized at 723 K (curve 2), and again reduced in $H_2$ at 673 K (curve 3), the same sample activated at 873 K and then reduced in $H_2$ at 673 K (curve 4). Each spectrum is reported after subtraction of the spectrum before CO admission and translated along the $Y$ axis for the sake of clarity.

cycling redox treatments were examined by using CO adsorption (see Fig. 8 for PdMgAl0.5(ac) as an example). The main differences observed on changing from the reduced (Fig. 8, curve 1) to the oxidized sample (Fig. 8, curve 2) were: (i) the presence of intense bands on the latter in the 1800–1000 $cm^{-1}$ region, assigned to carbonate-like species; (ii) the higher frequency of linear carbonyls (from 2076 to 2090 $cm^{-1}$ at the maximum CO coverage); (iii) the lower amount of bridge-bonded CO species; and (iv) the presence of small amounts of $Pd^+$ carbonyls (weak band at 2130 $cm^{-1}$). These findings account for a partial reduction of Pd oxide phase by CO at RT, most likely concerning only the surface and subsurface layers of PdO particles. As a consequence, electron donation from surface $Pd^0$ atoms to bulk $Pd^{2+}$ ions can occur in competition with the $\pi$ backdonation from surface $Pd^0$ to chemisorbed CO. This accounts for the observed increase of the frequency of linear carbonyls with respect to samples reduced in $H_2$. A different behavior was exhibited by the component at 2020 $cm^{-1}$, which maintains the same position despite the sample pretreatment, in line with the previous assignment to CO adsorbed on isolated Pd atoms. $CO_2$ formed upon PdO reduction was adsorbed on the basic support mainly as bidentate carbonates (1680–1570 $cm^{-1}$, $\nu$(C=O), 1350–1250, 1060–1040 $cm^{-1}$, $\nu_{asym}$, and $\nu_{sym}$ (OCO), respectively) and to minor extent as hydrogen carbonates (3616 $cm^{-1}$, $\nu$(OH); 1670, 1470 $cm^{-1}$, $\nu_{asym}$, and $\nu_{sym}$ (OCO), respectively; 1230 $cm^{-1}$, $\delta$(COH)). Note that, for the sake of clarity, in Fig. 8 we have restricted the spectroscopic region displayed to the high frequency modes of the carbonate-like species. These species were formed by interaction of $CO_2$ with the basic oxygen ions and hydroxyls of the support, respectively [29].

The spectra of CO adsorbed on the samples submitted to cycling reduction treatments were almost coincident (compare curves 1 and 3 in Fig. 8), indicating that Pd metallic and oxidic phases can be reversibly restored. At variance, some modifications in the nature of the metal phase occur when samples were activated at a higher temperature (873 K) before reduction in $H_2$ (Fig. 8, curve 4). Specifically, the bands due to linear carbonyls exhibited higher frequency, the band at 1960 $cm^{-1}$ assigned to 2-fold bridge-bonded species increased in intensity, while the one at 2020 $cm^{-1}$ decreased. All these findings put in evidence a decrease of the Pd dispersion. One can also note the increase of the band around 2200 $cm^{-1}$ due to $Al^{3+}$(CO), providing evidence of a surface enrichment in aluminum which is known to occur at high activation temperatures [21].

*3.3.1.3. Influence of the oxide support* The influence of the support, MgO, $Al_2O_3$, and Mg(Al)O, has been examined by CO adsorption for samples with low Pd loading (0.2 wt%, Figs. 9a and b) and high Pd loading (1.5 wt%, Fig. 9c only for MgO and Mg(Al)O-supported samples). The IR spectra call for several comments:

(i) On prereduced samples, the frequency of linear Pd carbonyls at low CO coverage has a similar value (ca. 2056 $cm^{-1}$) on PdMg0.2(ac) and PdMgAl0.2(ac), but it shifts to a higher frequency (ca. 2078 $cm^{-1}$) on PdAl0.2(ac). This feature indicates an increased electron density on Pd valence orbitals or a decrease in their ionization potential due the basic MgO and Mg(Al)O supports.

(ii) $Pd^+$(CO) species (2132 $cm^{-1}$) are clearly observed upon CO interaction with the oxidized PdAl0.2(ac) sample (Fig. 9a, curve 3), while bridged-bonded carbonyls and carbonates are formed in lower amounts with respect to PdMgAl0.2(ac). This accounts for the lower reducibility by CO of PdO when supported on $Al_2O_3$ in comparison to the other supports. Moreover, as already discussed, in the case of alumina-supported samples the band at ca. 2020–2015 $cm^{-1}$, assigned to Pd sites in strong interaction with the basic support, is absent (Figs. 9a and b, curve 3).

(iii) The bands of linear and bridged CO species (2090–2060 and 1975 $cm^{-1}$, respectively) on PdMg0.2(ac) (Figs. 9a and b, curve 1) are of lower intensity if compared with those on PdMgAl0.2(ac) (Figs. 9a and b, curve 2). Particularly, in the case of the prereduced PdMg0.2(ac) sample (Fig. 9b, curve 1) the intensity of carbonyl bands is negligible, while high amounts of carbonate-like species are unexpectedly formed.

The low amount of carbonyl species could indicate a lower dispersion or accessibility of Pd on the MgO support. Actually, the first hypothesis (low dispersion) is not consistent with HRTEM results, which suggest the presence of very small Pd clusters ($< 2$ nm). Moreover, carbonate formation on the prereduced sample points out to the occurrence of CO disproportionation (Boudouart reaction), with

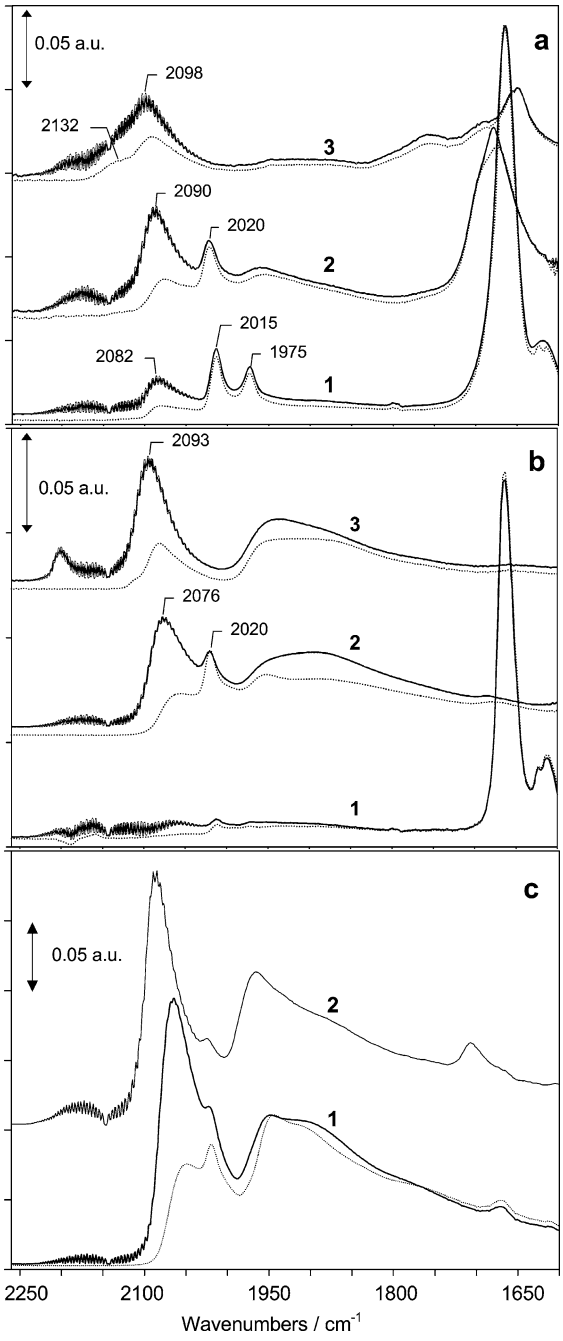


Fig. 9. Effect of the oxide support. IR spectra upon adsorption of CO (2 kPa) and subsequent evacuation (dotted lines) of samples oxidized at 723 K (a) or reduced in $H_2$ at 673 K (b and c). (a and b) PdMg0.2(ac) (curves 1), PdMgAl0.2(ac) (curves 2), PdAl0.2(ac) (curves 3). (c) PdMg1.5(ac) (curve 1), PdMgAl1.5(ac) (curve 2). Each spectrum is reported after subtraction of the spectrum before CO admission and translated along the *Y* axis for the sake of clarity.

C deposition on Pd and migration of $CO_2$ to basic sites. Carbon deposition can thus account for the low accessibility to Pd sites. Several authors reported that on small Pd clusters (< 4 nm) CO dissociation [43,50] or disproportionation [38,51] can occur, although at temperatures higher than those in our case. The higher intensity of carbonyl bands on the oxidized PdMg0.2(ac) sample indicates that the PdO phase, although partially reduced by CO at RT, has a low activity for the Boudouart reaction.

The peculiar activity of reduced PdMg0.2(ac) sample for CO disproportionation is not observed for all the Mg(Al)O and $Al_2O_3$-supported samples studied, nor for MgO-supported samples with higher Pd loadings. Indeed, by comparing the spectrum of prereduced PdMg1.5(ac) sample (Fig. 9c, curve 1) with that of PdMgAl1.5(ac) (Fig. 9c, curve 2) it is observed that linear and bridged carbonyls were formed in comparable amounts and no carbonates were formed. Therefore, the reactivity of Pd in the Boudouart reaction should arise from synergetic effects between very small particle sizes (< 2 nm) and/or particular particle shape and peculiar metal–support interactions.

### *3.3.2. Samples prepared by impregnation with $PdCl_2$*

The effects of the $PdCl_2$ precursor on the properties of the Pd phases depend first on the ability of the support in retaining chlorine, as previously discussed. Thus, as expected, significant differences were observed between PdMgAl$x$(Cl) and PdMgAl$x$(ac) catalysts, as seen in Fig. 10 where the spectra of high loading samples are compared. Specifically, upon CO admission on the oxidized PdMgAl1.2(Cl) sample (Fig. 10a, curve 1) a band with maximum at 2155 $cm^{-1}$, characteristic of $Pd^{2+}$ carbonyls, was observed, whereas $Pd^0$ carbonyls, both linear or bridged, and carbonate-like species were not formed. These findings are evidences of the difficulty of CO to reduce Pd ions in the presence of chlorine, suggesting that Pd is involved in supported palladium chloride or oxy-chloride species. In agreement, palladium(II) carbonyl halides are reported to have CO-stretching frequencies in the range 2200–2100 $cm^{-1}$ [52].

By comparing the reduced samples (Fig. 10b), one can remark on the higher CO-stretching frequencies (+15 $cm^{-1}$) of linear and bridged $Pd^0$ carbonyls on a PdMgAl1.2(Cl) sample (curve 1) with respect to PdMgAl1.5(ac) (curve 2), due to the electron-withdrawing effects of chlorine. Also observed is a lower linear/bridged CO species intensity ratio, accounting for a lower dispersion of the Pd phase, in agreement with HRTEM results reported above. Moreover, the peak at 2020 $cm^{-1}$ was absent. This reinforces the assignment of this band to CO chemisorbed on Pd sites strongly interacting with the basic oxygens sites of the support which are (partially or totally) depleted by chlorine. Finally, the higher intensity of the band around 2190 $cm^{-1}$ assigned to $Al^{3+}$–(CO) species accounts for a higher Lewis acidity of the PdMgAl1.2(Cl) sample with respect to PdMgAl1.5(ac).

A similar behavior is observed when comparing PdMgAl0.2(ac) (Figs. 9a and b, curves 2) and PdMgAl0.2(Cl) samples (Figs. 11a and b, curves 2). However, on the latter, the band at 2020 $cm^{-1}$ was not completely depleted, due to the lower chlorine content of this sample with respect to PdMgAl1.2(Cl).

Interestingly, the spectra of CO adsorbed on PdMgAl$x$(Cl) catalysts just activated or thereafter submitted to re-

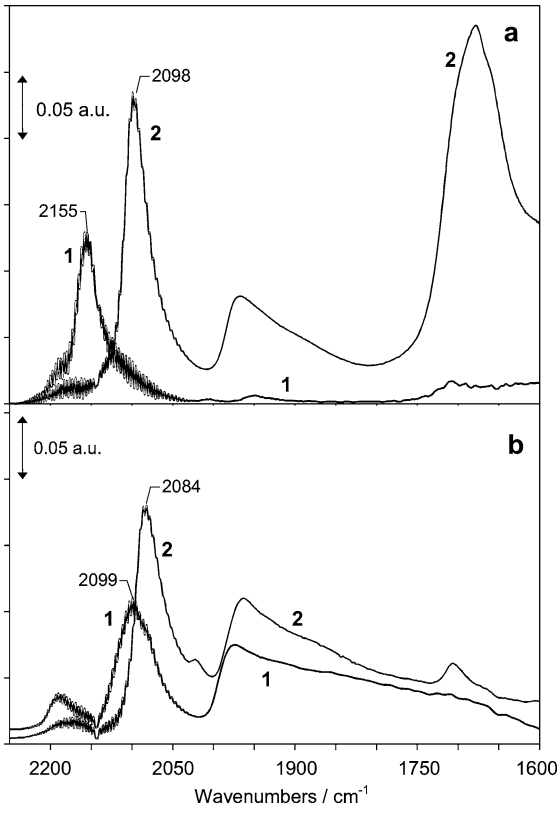


Fig. 10. Effect of the Pd precursor. IR spectra upon adsorption of CO (2 kPa) on PdMgAl1.2(Cl) (curves 1), and PdMgAl1.5(ac) (curves 2) samples oxidized at 723 K (a) or reduced in $H_2$ at 673 K (b). Each spectrum is reported after subtraction of the spectrum before CO admission.

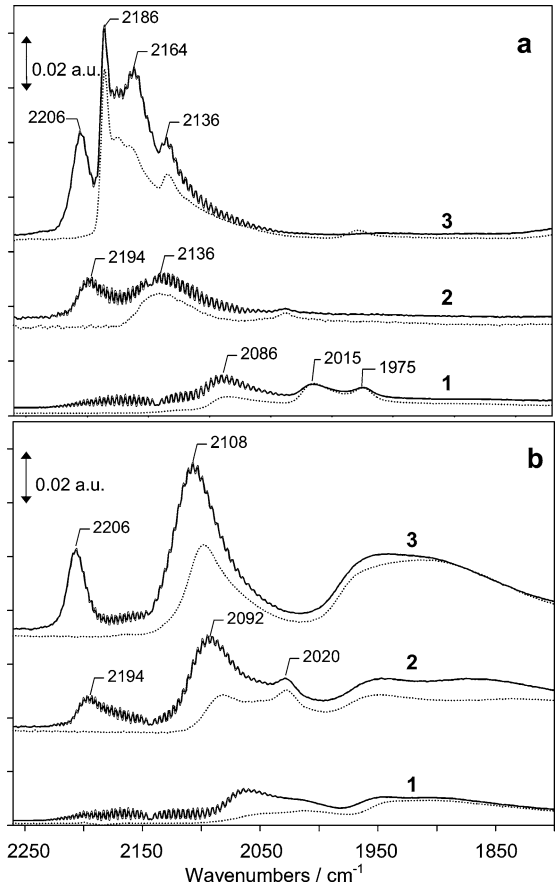


Fig. 11. Effect of the oxide support. IR spectra upon adsorption of CO (2 kPa) and subsequent evacuation (dotted lines) on PdMg0.2(Cl) (curves 1), PdMgAl0.2(Cl) (curves 2), PdAl0.2(Cl) (curves 3) samples oxidized at 723 K (a) or reduced in $H_2$ at 673 K (b). Each spectrum is reported after subtraction of the spectrum before CO admission and translated along the *Y* axis for the sake of clarity.

dox cycles superimposed quite nicely (not reported). These findings, along with the chemical analysis and the EDS data discussed above, suggest that Pd particles formed upon thermal reduction are completely surrounded by chlorine and that Pd oxy-chloride species are reversibly restored upon the subsequent reoxidation treatment.

As expected on the basis of the remaining Cl amounts, a significant influence of the $PdCl_2$ precursor is also observed in the case of the alumina-supported samples. In particular, the spectra of CO adsorbed on the oxidized PdAl0.2(Cl) sample (Fig. 11a, curve 3) were characterized by strong components at 2186, 2164, and 2136 $cm^{-1}$, assigned to CO stretching modes of $Pd^{2+}$ and $Pd^{+}$ carbonylhalide species, while carbonate-like species were not formed. Also in the case of the reduced PdAl0.2(Cl) sample (Fig. 11b, curve 3), the presence of chlorine induced a blue shift of the bands of linear and bridged carbonyls (from 2094 to 2108 $cm^{-1}$ and from 1937 to 1947 $cm^{-1}$, respectively, at full CO coverage) with respect to PdAl0.2(ac) sample. Again the higher intensity and frequency (from 2000 to 2206 $cm^{-1}$) of the band due to $Al^{3+}$(CO) species with respect to PdAl0.2(ac) sample account for the higher Lewis acidity induced by chlorine.

Finally, accounting for the very low Cl content in the MgO support, the spectra of the PdMg0.2(Cl) sample (Fig. 11, curves 1) were similar to those of PdMg0.2(ac) (Fig. 9, curves 1) and characterized by the very low intensities of the carbonyl bands and by the presence of high amounts of carbonates. These data suggest again that CO disproportionation reactions take place on MgO-supported samples with a low Pd loading.

## 4. Conclusions

Mg(Al)O mixed oxides obtained by thermal decomposition of hydrotalcite compounds have shown to be very attractive supports for the preparation of multifunctional Pd catalysts. These systems exhibit peculiar acid–base and metallic properties that can be finely tailored by varying the Pd loading and the nature of the Pd precursor used for the impregnation. In particular, the catalysts obtained using the acetylacetonate precursor show a strongly basic character, analogous to that of MgO, along with the presence of $Al^{3+}$ Lewis acid sites. The relative amounts of basic and acid sites are not significantly affected by the presence of palladium, while their absolute amounts decrease on samples with high Pd loading, due to the coverage of the mixed oxide surface.

CO adsorption experiments on catalysts obtained by $Pd(acac)_2$ have put in evidence peculiar interactions between the basic supports, Mg(Al)O and MgO, and the metal phases. Particularly, they reveal the presence of Pd sites, isolated or belonging to very small Pd clusters, strongly interacting with the basic oxygen anions of the support. These sites are responsible for a particular type of carbonyl species showing unusual features, such as the low stretching frequency, the low rate of formation, and the high stability.

Despite of the low $Al^{3+}$ content (relatively to $Mg^{2+}$) in the mixed oxides, the Mg(Al)O-supported Pd phases showed some properties which are more typical of Pd on alumina than on MgO, such as the low reactivity toward CO disproportionation or dissociation.

The impregnation with $PdCl_2$ has an effect on both acid–base properties and nature of Pd phases, which strictly depends on the nature of the oxide support and on its ability in retaining chlorine. Thus, negligible effects are observed in the case of MgO-supported samples, while the large amounts of remaining chlorine in alumina-supported samples account for the increase of the Lewis acid strength of the support, on the one hand, and for the presence of surface Pd chloride (or oxy-chloride) phases on the other hand. Although exhibiting a basic character similar to that of MgO, Mg(Al)O mixed oxides are able to retain significant amounts of chlorine as compensating anions of the layered structure. This accounts for the reconstruction of the hydrotalcite lamellar structure during the impregnation with the aqueous $PdCl_2$ solutions. Thus, the density of basic sites determined by $CH_3CN$ adsorption progressively decreases on increasing the Cl amounts, while the density and strength of the acid sites increase. CO adsorption reveals the presence of Pd oxy-chloride phases, while isolated Pd sites strongly interacting with the basic support are partially or totally depleted, depending on the chlorine concentration. Moreover, Pd particles obtained upon thermal reduction of the samples prepared using $PdCl_2$, showed larger average sizes and broader particle-size distributions with respect to those obtained from the acetylacetonate precursor.

## Acknowledgment

The authors gratefully acknowledge the Galileo Programme 2001–2003—Italian-French Integrated Actions—for financial support.

## References

[1] A. Vaccari, Appl. Clay Sci. 14 (1999) 161.
[2] F. Cavani, F. Trifirò, A. Vaccari, Catal. Today 11 (1991) 173.
[3] S. Ribet, D. Tichit, B. Coq, B. Ducourant, F. Morato, J. Solid State Chem. 142 (1999) 982.
[4] D. Tichit, S. Ribet, B. Coq, Eur. J. Inorg. Chem. 539 (2001).
[5] V. Rives, S. Kannan, J. Mater. Chem. 10 (2000) 489.
[6] V. Rives, F.M. Labajos, R. Trujillano, F. Romeo, C. Royo, A. Monzon, Appl. Clay Sci. 13 (1998) 363.
[7] F. Basile, G. Fornasari, M. Gazzano, A. Vaccari, Appl. Clay Sci. 16 (2000) 185.
[8] F. Trifirò, A. Vaccari, in: J.L. Atwood, J.E.D. Davies, D.D. Mac Nicol, F. Vögtle (Eds.), in: Comprehensive Supramolecular Chemistry, vol. 7, Pergamon, Oxford, 1996, pp. 251–291.
[9] D. Tichit, A. Vaccari (Eds.), Appl. Clay Sci. 13 (1998).
[10] Z. Gandao, B. Coq, L.C. de Ménorval, D. Tichit, Appl. Catal. A 147 (1996) 395.
[11] S.B. Sharma, J.T. Miller, J.A. Dumesic, J. Catal. 148 (1994) 198.
[12] F. Basile, G. Fornasari, M. Gazzano, A. Vaccari, Appl. Clay Sci. 18 (2001) 51.
[13] F. Basile, G. Fornasari, M. Gazzano, A. Kiennemann, A. Vaccari, J. Catal. 217 (2003) 245.
[14] Y.Z. Chen, C.W. Liaw, L.I. Lee, Appl. Catal. A 177 (1999) 1.
[15] F. Medina Cabello, D. Tichit, B. Coq, A. Vaccari, N.T. Dung, J. Catal. 167 (1997) 142.
[16] D. Tichit, R. Durand, A. Rolland, B. Coq, J. Lopez, P. Marion, J. Catal. 211 (2002) 511.
[17] J. Davis, E.G. Derouane, Nature 349 (1991) 313.
[18] Y.Z. Chen, C.M. Hwang, C.W. Liaw, Appl. Catal. A 169 (1998) 207.
[19] N. Das, D. Tichit, P. Graffin, B. Coq, Catal. Today 71 (2001) 181.
[20] M. Martinez Ortiz, D. Tichit, P. Gonzales, B. Coq, J. Mol. Catal. A, in press.
[21] F. Prinetto, G. Ghiotti, P. Graffin, D. Tichit, Micropor. Mesopor. Mater. 39 (2000) 229.
[22] F. Prinetto, G. Ghiotti, R. Durand, D. Tichit, J. Phys. Chem. B 104 (2000) 11117.
[23] V.B. Kazanski, V.Yu. Borovkov, A.I. Serykh, F. Figueras, Catal. Lett. 49 (1997) 35.
[24] B. Rebours, J.B. d'Espinose de la Caillerie, O. Clause, J. Am. Chem. Soc. 116 (1994) 1707.
[25] N. Mahata, V. Vishwanathan, J. Catal. 196 (2000) 262.
[26] H. Knözinger, H. Krietenbrink, J. Chem. Soc., Faraday Trans. I 71 (1975) 2421.
[27] J. Yarwood, in: Spectroscopy and Structure of Molecular Complexes, Plenum, London, 1973, p. 141.
[28] K.F. Purcell, R.S. Drago, J. Am. Chem. Soc. 88 (1966) 919.
[29] J.C. Lavalley, Catal. Today 27 (1996) 377.
[30] C. Binet, A. Jadi, J.C. Lavalley, J. Chim. Phys. 89 (1992) 31.
[31] V.R.L. Constantino, T.J. Pinnavaia, Inorg. Chem. 34 (1995) 883.
[32] I.C. Chisem, W. Jones, I. Martin, C. Martin, V. Rives, J. Mater. Chem. 8 (1998) 1917.
[33] R.P. Eischens, W.A. Pliskin, Adv. Catal. 10 (1958) 1.
[34] N. Sheppard, C. De La Cruz, Catal. Today 70 (2001) 3.
[35] A.M. Bradshaw, F.M. Hoffmann, Surf. Sci. 72 (1978) 513.
[36] A. Ortega, F.M. Hoffmann, A.M. Bradshaw, Surf. Sci. 119 (1982) 79.
[37] W.K. Kuhn, J. Szanyi, D.W. Goodman, Surf. Sci. Lett. 274 (1992) L611.
[38] S. Ichikawa, H. Poppa, M. Boudart, J. Catal. 91 (1985) 1.
[39] R. van Hardeveld, F. Hartog, Adv. Catal. 72 (1972) 75.
[40] C. Binet, A. Jadi, J.C. Lavalley, J. Chim. Phys. 86 (1989) 451.
[41] C. Binet, A. Jadi, J.C. Lavalley, M. Boutonnet-Kizling, J. Chem. Soc., Faraday Trans. 88 (1992) 2079.
[42] C.R. Henry, C. Chapon, C. Goyhenex, R. Monot, Surf. Sci. 272 (1992) 283.
[43] E. Gillet, S. Channakhone, V. Matolin, J. Catal. 97 (1986) 437.
[44] A. Badri, C. Binet, J.C. Lavalley, J. Chim. Phys. 92 (1995) 1333.
[45] W.T. Reichle, S.Y. Kang, D.S. Everhardt, J. Catal. 101 (1986) 352.
[46] B.L. Mojet, J.T. Miller, D.E. Ramaker, D.C. Koningsberger, J. Catal. 186 (1999) 373.
[47] D.E. Ramaker, J. de Graaf, J.A.R. van Veen, D.C. Koningsberger, J. Catal. 203 (2001) 7.
[48] S. Abbet, E. Riedo, H. Brune, U. Heiz, A.M. Ferrari, L. Giordano, G. Pacchioni, J. Am. Chem. Soc. 123 (2001) 6172.
[49] J. Raskó, J. Catal. 217 (2003) 478.
[50] D.L. Doering, H. Poppa, J.T. Dickinson, J. Catal. 73 (1982) 104.
[51] V. Matolin, E. Gillet, Surf. Sci. 238 (1990) 75.
[52] K.I. Choi, M.A. Vannice, J. Catal. 127 (1991) 465.